



Promoting effect of Mn and Ti on the structure and performance of Co₃O₄ catalysts for oxidation of dibromomethane



Jian Mei, Zan Qu, Songjian Zhao, Xiaofang Hu, Haomiao Xu, Naiqiang Yan*

School of Environmental Science and Engineering, Shanghai Jiao Tong University, 800 Dong Chuan Road, Shanghai 200240, PR China

ARTICLE INFO

Article history:

Received 7 June 2017

Received in revised form 11 August 2017

Accepted 15 August 2017

Available online 24 August 2017

Keywords:

Dibromomethane
Catalytic oxidation
Co₃O₄
Mn
Ti

ABSTRACT

Co₃O₄ catalysts modified with Mn and Ti, prepared by co-precipitation method, were used for catalytic oxidation of dibromomethane (CH₂Br₂), a model molecule for brominated volatile organic compounds (BVOCs). Addition of Ti or Ti + Mn distorted the crystal structure and led to the formation of a Co–O–Ti solid solution. The addition of Mn further enhanced the surface acidity and redox ability of the catalysts. Co–Mn–Ti exhibited the highest activity with a T₉₀ of approximately 234 °C and the highest selectivity to CO₂ at low temperatures. Additionally, Co–Mn–Ti showed good stability for at least 30 h at 500 ppm CH₂Br₂, 0 or 2 vol% H₂O, 0 or 500 ppm *p*-xylene (PX), and 10% O₂ at a gas hourly space velocity of 60,000 h⁻¹, and the final products were CO_x, Br₂, and HBr, without the formation of other Br-containing organic byproducts. This high catalytic activity was attributed to its high specific area, high surface acidity, and strong redox property. Furthermore, the synergetic effect of Co, Mn, and Ti made it superior for CH₂Br₂ oxidation. A plausible reaction mechanism for CH₂Br₂ oxidation over Co–Mn–Ti catalysts was proposed based on the analysis of the products and *in situ* diffuse-reflectance infrared Fourier transform spectroscopy results.

© 2017 The Korean Society of Industrial and Engineering Chemistry. Published by Elsevier B.V. All rights reserved.

Introduction

With increasingly strict air pollutant emission standards implemented by environmental legislation, there is increasing concern over the abatement of halogenated volatile organic compounds (HVOCs) owing to their direct harmful effects on the environment and human health [1–3]. Brominated volatile organic compounds (BVOCs) are emitted by several different sectors, including the petrochemical and pharmaceutical industries. BVOCs are typically released from purified terephthalic acid (PTA) exhaust gas, and their disposal is both an urgent concern and a challenge owing to their resistance to degradation [4]. Thermal oxidation is conventionally used for the treatment of BVOCs at high concentrations. This usually requires temperatures higher than 1000 °C necessitating the use of additional fuel. In addition, incomplete thermal oxidation of BVOCs can produce undesirable byproducts. Catalytic oxidation is an economically efficient technology for the oxidation of BVOCs to CO₂, H₂O, and other less harmful compounds at a relatively low temperature and is recognized as one of the most promising technologies for the

abatement of BVOCs owing to its low energy consumption and high efficiency [5].

At present, the catalysts used for BVOCs oxidation are mainly classified into two groups: noble metals [6] and transition metal oxides [7]. Noble metal catalysts show excellent catalytic activity but tend to yield multi-brominated byproducts and undergo deactivation due to Br adsorption. Transition metal oxides have been increasingly explored as catalysts for BVOCs oxidation owing to their low cost and high thermal stability, such as Fe₂O₃/Al₂O₃ [8], CuO/CeO₂-Al₂O₃ [8], and Ce–Mn mixed oxide [9]. However, their low activity remains a problem. Hence, considerable research effort has been dedicated to improving their catalytic activity.

Among transition metal oxides, Co₃O₄ is one of the most efficient catalysts for BVOCs oxidation because of its highly mobile oxygen content and excellent reduction ability, as well as its high concentration of electrophilic oxide species [10,11]. Although Co₃O₄ is easily deactivated due to the formation of brominated species at its surface, its ability to resist Br poisoning can be promoted by the addition of other elements [7]. Furthermore, its redox ability can also be enhanced on combination with other elements [12]. Manganese oxides (MnO_x) as structural-promoting components exhibit various valence states and high efficiency in reaction/oxidation cycles [13,14]. Furthermore, Co–Mn mixed oxide catalysts have been proven to exhibit high catalytic activity

* Corresponding author. Fax: +86 21 54745591.

E-mail address: nqyan@sjtu.edu.cn (N. Yan).

for 1,2-dichlorobenzene and methane oxidation [15,16]. Moreover, titania (TiO₂) as an environmentally friendly material has been widely explored as an agent for VOCs oxidation owing to its strong acidity and unique redox behavior [17,18]. Thus, the incorporation of Mn and Ti into Co₃O₄ presents a feasible strategy for the preparation of novel catalysts with high performance for BVOCs oxidation.

In this study, Co₃O₄, Co–Mn, Co–Ti, and Co–Mn–Ti mixed oxide catalysts were prepared by co-precipitation method, and were used in the catalytic oxidation of dibromomethane (CH₂Br₂), which was selected as a model molecule for BVOCs. Several new perspectives regarding Co–Mn–Ti mixed oxide catalysts for catalytic oxidation of BVOCs were suggested, and the relationship between the catalytic performance and structural features of the catalysts was also investigated.

Experimental

Catalyst preparation

The Co–Mn–Ti mixed oxide catalyst was prepared by co-precipitation method. The appropriate amount of Ti(OC₄H₉)₄ was dissolved in 40 mL C₂H₅OH under magnetic stirring to form solution A. Then, appropriate amounts of Co(NO₃)₂·6H₂O and/or Mn(NO₃)₂ were dissolved in 50 mL H₂O under magnetic stirring to form solution B (Co:Ti:Mn = 20:5:1). Next, solution B was added dropwise into solution A, and 10 mL NH₃·H₂O was added dropwise into the resulting mixed solution under magnetic stirring and the solution was stirred for a further 3 h. The obtained precipitates were isolated by filtering and washed three times in ultrapure water. After drying at 90 °C for 10 h, the precipitates were calcined at 500 °C for 3 h in air. Co₃O₄, MnO_x, TiO₂, Co–Mn (Co:Mn = 20:1), and Co–Ti (Co:Ti = 4:1) catalysts were prepared by the same method, and used as reference samples.

Catalyst characterization

The power X-ray diffraction (XRD) patterns were recorded on a Shimadzu XRD-6100, and the diffractograms were collected in the 2θ range of 10–80° with a scanning velocity of 10°/min. The nitrogen adsorption and desorption isotherms were measured using a physical adsorption instrument (Nova 2200e) at –196 °C. The samples were outgassed in vacuum at 200 °C for 3 h before the measurement. The specific surface area was calculated using the multi-point Brunauer-Emmett-Teller (BET) model, and pore size and pore volume were calculated using the Barrett-Joyner-Halenda (BJH) model. Raman spectra were carried out on a SENTERRA R200 microscope. The excitation source was the 532 nm line of Ar ion laser. The X-ray photoelectron spectroscopy (XPS) was carried out on a PHI-5300 (PE) spectrometer using Mg Kα radiation as an excitation source, and the binding energy was calibrated using the C 1s line at 284.8 eV as an internal standard. The H₂-temperature-programmed reduction (H₂-TPR) experiments were carried out on a chemical adsorption instrument (AutoChem II, 2920). Before the analysis, the 50 mg samples were pretreated in Ar flow at 300 °C for 2 h. Then, after cooling to 100 °C, the samples were heated to 1000 °C in 10% H₂/Ar flow at a heating rate of 10 °C/min. The NH₃-temperature-programmed desorption (NH₃-TPD) experiments were also carried out on a chemical adsorption instrument (AutoChem II, 2920). Before the analysis, the 300 mg samples were pretreated in He flow at 300 °C for 2 h. Then, after cooling to 50 °C, NH₃ adsorption was carried out in 10% NH₃/He flow at 50 °C for 1 h. Subsequently, the samples were treated in He flow for 30 min to remove physically adsorbed NH₃, and then heated to 800 °C in He flow at a heating rate of 10 °C/min.

Catalytic activity measurement

Catalytic oxidation of CH₂Br₂ was conducted on a fixed-bed quartz tube reactor with an inner diameter of 6 mm. The reaction temperatures investigated were in the range of 150–300 °C. The catalyst samples (80 mg) were sandwiched between two silica wool layers in the middle of the reactor. The total gas flow was 150 mL min^{–1} corresponding to a gas hourly space velocity (GHSV) of 60,000 h^{–1}. The simulated gas generally comprised 500 ppm CH₂Br₂, 10% O₂, 500 ppm *p*-xylene (PX) (when used), 2 vol% H₂O (when used), and N₂ as the balance. The gaseous CH₂Br₂ was produced by a N₂ flow through a bottle containing pure CH₂Br₂ liquid in a homoiothermal oil bath. The gaseous PX and H₂O were produced by the same method. The CH₂Br₂ concentrations in the inlet and outlet were determined by a GC-2010 Plus gas chromatographer fitted with a flame ionization detector (FID) and were collected at each investigated temperature after allowing the system to stabilize for 30 min. The catalytic activity was evaluated in accordance with CH₂Br₂ conversion, defined as follows:

$$X_{\text{CH}_2\text{Br}_2} = \frac{C_{\text{in}} - C_{\text{out}}}{C_{\text{in}}} \times 100\% \quad (1)$$

where C_{in} and C_{out} are the CH₂Br₂ concentrations corresponding to the inlet and outlet, respectively.

The gas products in the outlet were detected by a GCMS-QP2010. The concentrations of HBr and Br₂ were monitored by the titration method. Firstly, the gas flow containing HBr and Br₂ was fully absorbed in a KI solution. Secondly, the concentration of Br₂ was monitored by titration using Na₂S₂O₃ solution with starch solution as an indicator. The concentration of bromide ions in the absorbed solution was monitored by an ion chromatography. The concentrations of CO and CO₂ were determined by a GC-14B gas chromatographer fitted with a FID and a methane conversion oven. The selectivity to CO, CO₂, HBr, and Br₂ were defined as follows, respectively:

$$S_{\text{CO}} = \frac{C_{\text{CO}}}{C_{\text{in}} - C_{\text{out}}} \times 100\% \quad (2)$$

$$S_{\text{CO}_2} = \frac{C_{\text{CO}_2}}{C_{\text{in}} - C_{\text{out}}} \times 100\% \quad (3)$$

$$S_{\text{HBr}} = \frac{C_{\text{HBr}}}{2(C_{\text{in}} - C_{\text{out}})} \times 100\% \quad (4)$$

$$S_{\text{Br}_2} = \frac{C_{\text{Br}_2}}{C_{\text{in}} - C_{\text{out}}} \times 100\% \quad (5)$$

where C_{CO} and C_{CO_2} are the concentrations of CO and CO₂ (ppm) in the outlet, C_{HBr} and C_{Br_2} are the concentrations of Br₂ and HBr (ppm) in the outlet.

In situ DRIFTS study

In situ diffuse-reflectance infrared Fourier transform (DRIFT) spectroscopy experiments were performed on a Fourier transform infrared spectrometer (FTIR, Nicolet 6700) fitted with a MCT detector. The DRIFTS cell was fitted with ZnSe windows and a heating chamber. The real reaction conditions were simulated by a temperature controller and mass flow controllers. Spectra were collected in the range of 4000–800 cm^{–1} at a resolution of 4 cm^{–1} and over 100 scans. Prior to each experiment, the samples were

pretreated with 10% O₂/N₂ at 400 °C for 2 h to purify catalyst surface, and then cooled to 50 °C. Spectra of the clean catalyst surface were collected at each evaluated temperature and used as the background. Next, a gas flow containing 500 ppm CH₂Br₂/10% O₂/N₂ was exposed to the DRIFTS cell at 50 °C for 1 h. Finally, the catalyst was treated in 10% O₂/N₂ from 50 to 350 °C, and the spectra were collected from 50 to 350 °C.

Results and discussion

Catalytic performance

Conversion curves for CH₂Br₂ oxidation over Co–Ti prepared with different Co/Ti ratios are shown in Fig. S1, and CH₂Br₂ conversion over Mn-modified Co–Ti catalysts prepared with different Co/Mn ratios are shown in Fig. S2. The results show that Co–Mn–Ti (Co:Mn:Ti=20:5:1) exhibits the highest catalytic activity. Conversion curves for CH₂Br₂ oxidation over Co₃O₄, MnO_x, TiO₂, Co–Mn, Co–Ti, and Co–Mn–Ti catalysts are shown in Fig. 1. Pure Co₃O₄ exhibits high activity with a T₉₀ (the temperature needed for 90% conversion) of approximately 287 °C. With the addition of Mn, the catalytic activity of Co₃O₄ increases and conversion curves shift to lower temperature, with a T₉₀ of approximately 267 °C. Moreover, Co–Ti and Co–Mn–Ti are superior for CH₂Br₂ oxidation, and their T₉₀ values are approximately 245 and 234 °C, respectively, which are lower than those of Co–Mn and Co₃O₄. The results reveal that Ti plays an important role in the improvement of catalytic activity, and that Mn exhibits a synergistic effect. However, MnO_x is lower activity than Co₃O₄, and its T₉₀ value is approximately 296 °C. TiO₂ has the lowest activity, and the CH₂Br₂ conversion is only 36.6% at 300 °C. Thus, based on the T₉₀ values, the order of the catalytic activity for CH₂Br₂ oxidation is Co–Mn–Ti > Co–Ti > Co–Mn > Co₃O₄ > MnO_x > TiO₂. Furthermore, our work is compared with those recently reported in literatures, and the results are listed in Table 1. It is found that the catalytic activity of Co–Mn–Ti is superior to all the

catalysts listed, such as CoTi-5 [10], Mn–Co/TiO₂ [7] and Co₃O₄/CeO₂-rod [19].

Catalyst characterization

The XRD patterns of Co₃O₄, Co–Mn, Co–Ti, and Co–Mn–Ti catalysts are shown in Fig. 2, revealing that Mn and Ti have significant effects on the crystallinity of the catalysts. Pure Co₃O₄ presents eight intense and sharp peaks at 19.0, 31.3, 36.8, 38.6, 44.8, 55.7, 59.4, and 65.3°, which can be indexed to spinel structure Co₃O₄ [20]. With the addition of Mn or Ti, the diffraction peaks for spinel Co₃O₄ become weaker and broader and no new diffraction peaks appeared. By calculating the Scherrer equation applied for (3 1 1), the crystalline particle size decreased from 28.4 nm for pure Co₃O₄ to 20.9, 12.8, and 12.1 nm for Co–Mn, Co–Ti and Co–Mn–Ti, respectively (Table 2), suggesting a decrease in the size of the spinel Co₃O₄ particles. Many other studies have demonstrated that Mn_xCo_{3–x}O₄ and Ti_xCo_{3–x}O₄ solid solutions with spinel structures can be prepared by the co-precipitation method [21,22].

The N₂ adsorption–desorption isotherms and pore-size distributions of Co₃O₄, Co–Mn, Co–Ti, and Co–Mn–Ti catalysts are shown in Fig. S3, and their physical properties as estimated by N₂ physisorption are listed in Table 2. As shown in Fig. S3(a), the N₂ adsorption–desorption isotherms of all the samples may be assigned as type IV with a type H3 hysteresis loop at high relative pressure. As shown in Fig. S3(b), the pore sizes in pure Co₃O₄ are in the range 10–60 nm, as calculated from its N₂ adsorption–desorption isotherm used the BJH model, and the average pore diameter is 23.02 nm. For Co–Mn, the pore diameter is almost unchanged. However, the pore sizes for both Co–Ti and Co–Mn–Ti are around 3 nm. This result reveals that the addition of Ti remarkably decreases the pore size of the catalysts. Moreover, as can be seen in Table 2, the specific surface area of Co₃O₄ is only 0.2 m² g^{–1}, and that of Co–Mn is improved to 31.7 m² g^{–1}. Furthermore, the specific surface area of Co₃O₄ is greatly improved by addition of Ti, with those of Co–Ti and Co–Mn–Ti being 46.3 and 64.6 m² g^{–1}, respectively. Among the four catalysts investigated, the specific surface area of Co–Mn–Ti is the largest. These results reveal that Ti plays an important role in improving the specific surface area of the catalysts, and that Mn exhibits a synergistic effect.

To further confirm the lattice structural distortion of the catalyst, Raman spectroscopy was conducted, and the results are shown in Fig. 3. In the wavenumber range 100–800 cm^{–1}, pure Co₃O₄ presents five well-defined Raman-active modes: F_{2g} (192, 513, and 611 cm^{–1}), E_g (472 cm^{–1}) and A_{1g} (678 cm^{–1}), which can be

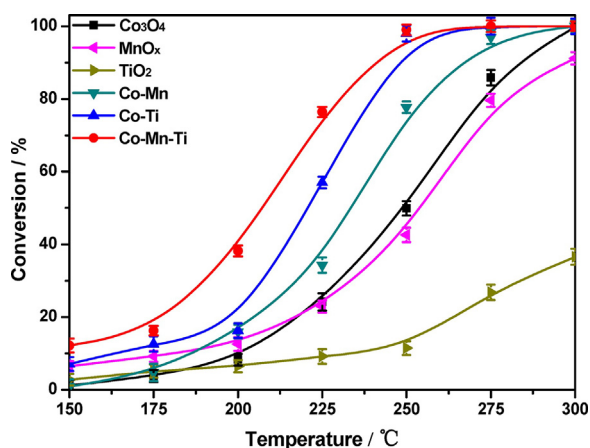


Fig. 1. Conversion curves for CH₂Br₂ oxidation over Co₃O₄, MnO_x, TiO₂, Co–Mn, Co–Ti, and Co–Mn–Ti catalysts; operating condition: 500 ppm CH₂Br₂, 10% O₂, and N₂ balance; GHSV = 60,000 h^{–1}.

Table 1
Some work made on oxidation of CH₂Br₂ with transition metal oxide catalysts.

Catalyst	CH ₂ Br ₂ /ppm	GHSV	T ₉₀ /°C
CoTi-5	500	60,000 h ^{–1}	346
Mn–Co/TiO ₂	500	60,000 h ^{–1}	325
Co ₃ O ₄ /CeO ₂ -rod	500	75,000 mL/(g h) ^{–1}	312
Co–Mn–Ti	500	60,000 h ^{–1}	234

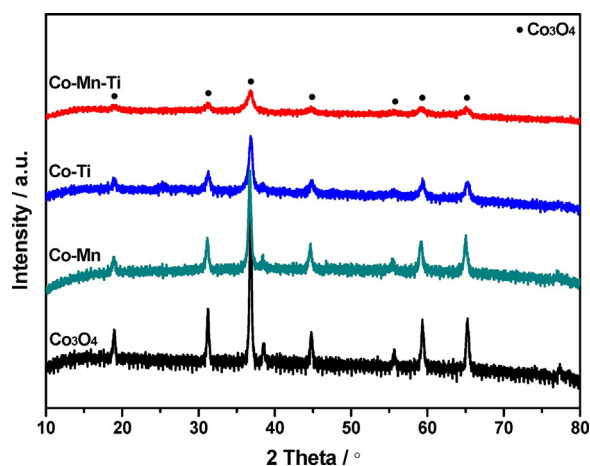


Fig. 2. XRD patterns of Co₃O₄, Co–Mn, Co–Ti, and Co–Mn–Ti catalysts.

Table 2
Physical properties of Co₃O₄, Co–Mn, Co–Ti, and Co–Mn–Ti catalysts.

Catalyst	S _{BET} (m ² g ⁻¹)	Average pore diameter (nm)	Average pore volume (cm ³ g ⁻¹)	D _{Co3O4} (nm)
Co ₃ O ₄	0.2	23.02	0.02	28.4
Co–Mn	31.7	23.46	0.21	20.9
Co–Ti	46.3	3.59	0.15	12.8
Co–Mn–Ti	64.6	3.63	0.15	12.1

D_{Co3O4}: Co₃O₄ crystallite size calculated by Scherrer equation from XRD.

attributed to spinel structure Co₃O₄ [23]. The F_{2g} and E_g modes correspond to the vibrations of tetrahedral and octahedral sites, respectively, while the A_{1g} mode is related to the occurrence of octahedral sites. The addition of Mn shifts the Raman peaks of Co₃O₄ to lower frequencies and make them more asymmetric and broader. This could be due to lattice distortion or structural disorder of the spinel Co₃O₄. In the case of Co–Ti, the peaks attributed to spinel Co₃O₄ basically disappear and new bands at 225, 257, 326, 376, and 688 cm⁻¹ are observed. The first four bands correspond to Co₂TiO₄ [24], and the last to CoTiO₃ [25]. This confirms that Co–O–Ti solid solutions have formed. It is interesting to note that the Raman peaks for Co–Mn–Ti are similar to those for Co–Ti, except that weak peaks attributed to spinel Co₃O₄ appear and the peaks are slightly shifted to higher frequencies, suggesting interactions between Co, Mn, and Ti and the possibility of the formation of Co–O–Mn–O–Ti solid solutions.

To investigate the surface chemical composition and oxidation state of the catalyst, XPS was conducted, and the results are shown in Fig. 4 and Table 3. As shown in Fig. 4(a), two main peaks (with satellite peaks) assigned to Co 2p_{3/2} and Co 2p_{1/2} at 775–785 eV and 791–801 eV, respectively, are observed for all samples. The main Co 2p_{3/2} spectra can be further resolved into two components with a binding energy (BE) centered at 778.7–780.4 eV and 779.8–781.6 eV. The peak with a BE at 778.7–780.4 eV corresponds to Co³⁺, whereas the peak with a BE at 779.8–781.6 eV is related to Co²⁺ [26]. Furthermore, the satellite peak also confirms the presence of Co²⁺ in the catalysts. As shown in Table 3, for Co₃O₄, the ratio of Co³⁺/Co²⁺ is 0.30. The addition of Ti into Co₃O₄ causes the ratio of Co³⁺/Co²⁺ to increase to 1.02, indicating that some Co ions are oxidized from Co²⁺ to Co³⁺ as Ti species entered the spinel structure, and that most Ti species substitute for Co²⁺ in the tetrahedral sites. However, for Co–Mn–Ti, the ratio of Co³⁺/Co²⁺ is lower than that in Co–Ti, implying that most Mn species substitute for Co³⁺ in the octahedral sites owing to the presence of Ti.

In the O 1s spectra (Fig. 4(b)), the asymmetric peak can be divided into two components. The one with a BE at 529.8–529.0 eV corresponds to lattice oxygen (O_{ads}), and the other with a BE at

529.5–530.1 eV is related to surface-adsorbed oxygen (O_{ads}) [27]. The areal ratio of O_{ads}/O_{lat} reflects the proportion of the two different oxygen species, and a higher ratio indicates a larger amount of chemisorbed oxygen species. As shown in Table 3, the O_{ads}/O_{lat} ratio for Co₃O₄ is higher than that of the other catalysts, and Co–Mn–Ti has the lowest O_{ads}/O_{lat} ratio. These results imply that the addition of Mn and Ti into Co₃O₄ inhibits the formation of surface adsorbed oxygen.

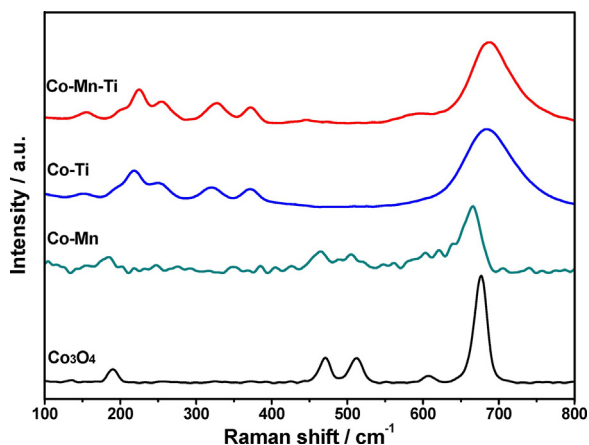


Fig. 3. Raman spectra of Co₃O₄, Co–Mn, Co–Ti, and Co–Mn–Ti catalysts.

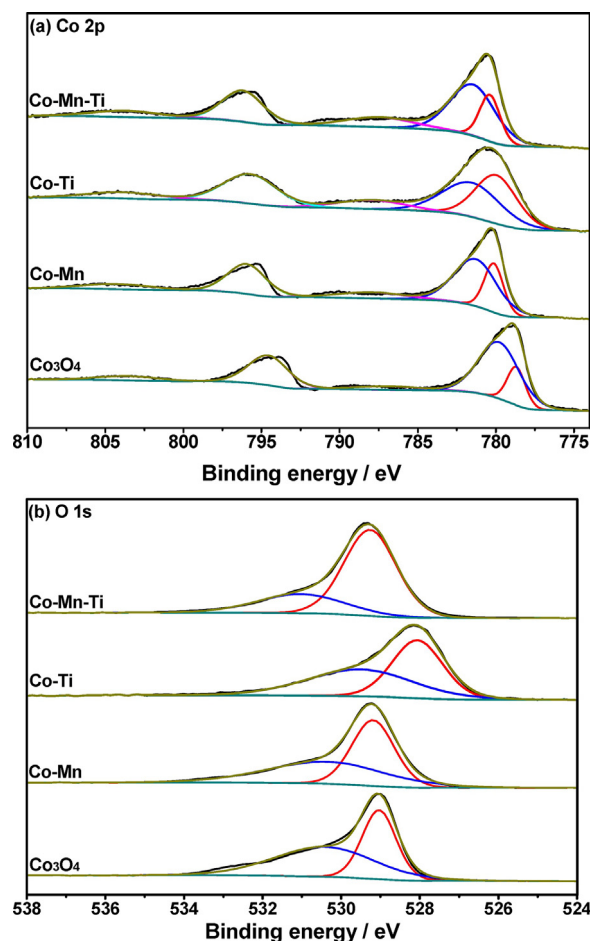


Fig. 4. XPS spectra of Co 2p (a) and O 1s (b) for Co₃O₄, Co–Mn, Co–Ti, and Co–Mn–Ti catalysts.

Table 3
XPS parameters of Co₃O₄, Co–Mn, Co–Ti, and Co–Mn–Ti catalysts.

Catalyst	Co (at.%)	Mn (at.%)	Ti (at.%)	Co ³⁺ /Co ²⁺	O _{ads} /O _{lat}
Co ₃ O ₄	15.61	–	–	0.30	1.27
Co–Mn	14.66	7.17	–	0.46	0.93
Co–Ti	14.50	–	4.95	1.02	0.96
Co–Mn–Ti	13.21	3.63	7.21	0.41	0.37

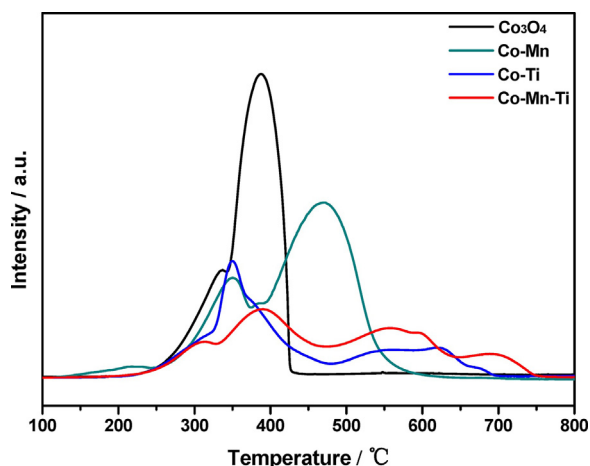


Fig. 5. H_2 -TPR profiles of Co_3O_4 , Co-Mn, Co-Ti, and Co-Mn-Ti catalysts.

The reducibility of the catalysts is evaluated by H_2 -TPR, and the results are shown in Fig. 5. The H_2 -TPR profile of Co_3O_4 shows two overlapping reduction peaks centered at 337 and 387 °C. It is reasonable to assume that the peak at low temperature can be ascribed to the reduction of Co^{3+} to Co^{2+} , and that the peak at high temperature is related to the reduction of Co^{2+} to Co^0 [28]. With the addition of Mn to Co_3O_4 , three reduction peaks centered at 218, 350, and 471 °C are observed. The first shoulder peak corresponds to the reduction of Mn_2O_3 to Mn_3O_4 or $CoMnO_3$ [15], while the second and third peak might be assigned to the reduction of Co^{3+} to Co^{2+} and Co^{2+} to Co^0 , respectively. Compared with pure Co_3O_4 , the reduction peaks of Co-Ti are shifted to higher temperature. The possible reason for this is that, on one hand, Ti^{4+} substitutes for Co^{3+} in the octahedral sites of Co_3O_4 , and on the other hand, the formation of Co-O-Ti in the spinel Co_3O_4 results in a decrease of oxidation ability. For Co-Mn-Ti, five reduction peaks centered at 314, 390, 559, 594, and 688 °C are observed. The former two peaks correspond to Co^{3+} to Co^{2+} and Co^{2+} to Co^0 reductions, respectively, while the latter three peaks may be assigned to a Co-O-Ti solid solution or TiO_2 . The results reveal that Mn plays a significant role in promoting the reducibility of the catalysts, and that Ti has a synergistic effect.

It has been reported that the surface acidic properties of a catalyst play a significant role in VOCs oxidation because they dictate the nature of active sites for the adsorption of VOCs molecules. These properties were investigated by NH_3 -TPD, and the results are shown in Fig. 6. Co_3O_4 presents two desorption

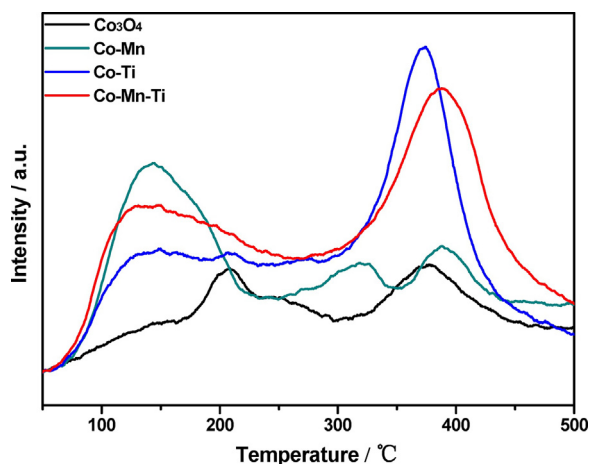


Fig. 6. NH_3 -TPD profiles of Co_3O_4 , Co-Mn, Co-Ti, and Co-Mn-Ti catalysts.

peaks, which are attributed to NH_3 desorbed from weak and strong acid sites. However, three desorption peaks are observed for Co-Mn, corresponding to NH_3 desorbed from weak, moderated, and strong acid sites. The desorption peak related to weak acid sites is shifted to lower temperature and the amount of NH_3 desorption is also clearly increased. Two broad desorption peaks are observed for Co-Ti. The desorption peak related to weak acid sites is shifted to lower temperature, and the amount of NH_3 desorption corresponding to strong acid sites is significantly increased. Co-Mn-Ti presents the lowest desorption peak temperature and the largest amount of NH_3 desorption. These results indicate that the addition of Mn promotes the formation of weak acid sites, and the addition of Ti facilitates the formation of strong acid sites, which favor CH_2Br_2 oxidation.

Analysis of products

As is well known, the desired products from the oxidation of brominated hydrocarbons are CO_2 , HBr, and Br_2 . However, some byproducts, such as CO and unwanted Br-containing organic compounds, are often generated in the process of oxidation. Therefore, it is necessary to investigate product composition and selectivity to the desired products when developing a catalytic oxidation process. Tables 4 and 5 show the oxidation products over Co_3O_4 and Co-Mn-Ti as detected by GC-MS. The oxidation products are CO, CO_2 , HBr, Br_2 , and H_2O , and no other Br-containing organic byproducts are detected. However, the product selectivity is different, depending on the catalyst used, and the selectivities to CO, CO_2 , HBr, and Br_2 as a function of temperature over Co_3O_4 and Co-Mn-Ti are shown in Fig. 7. For pure Co_3O_4 , the selectivities to CO and HBr gradually decrease with increasing temperature, while those to CO_2 and Br_2 gradually increase. Similar phenomena are also observed for Co-Mn-Ti. The selectivity to CO_2 is approximately 23% and 61% at 150 and 200 °C, respectively, and is 100% above 250 °C. This increase in selectivity to CO_2 is ascribed to the increased oxidation of CO at higher temperature. Furthermore, Br_2 is generated when the temperature exceeds 175 °C, which can be ascribed to the Deacon reaction ($4HBr + O_2 \rightarrow 2Br_2 + 2H_2O$) [29]. The selectivity to Br_2 reaches 61% at 300 °C. For Co-Mn-Ti, the selectivity to CO_2 is 41 and 82% at 150 and 200 °C, respectively, which is higher than that with Co_3O_4 , and is 100% above 225 °C. In addition, Br_2 is generated when the temperature is only 150 °C, and the selectivity to Br_2 is higher than that with Co_3O_4

Table 4
Products in outlet at different temperature over Co_3O_4 .

Temperature (°C)	Detected substances
150	CH_2Br_2 , CO, CO_2 , HBr, H_2O
175	CH_2Br_2 , CO, CO_2 , Br_2 , HBr, H_2O
200	CH_2Br_2 , CO, CO_2 , Br_2 , HBr, H_2O
225	CH_2Br_2 , CO, CO_2 , Br_2 , HBr, H_2O
250	CH_2Br_2 , CO_2 , HBr, Br_2 , H_2O
275	CH_2Br_2 , CO_2 , HBr, Br_2 , H_2O
300	CH_2Br_2 , CO_2 , HBr, Br_2 , H_2O

Table 5
Products in outlet at different temperature over Co-Mn-Ti.

Temperature (°C)	Detected substances
150	CH_2Br_2 , CO, CO_2 , HBr, H_2O
175	CH_2Br_2 , CO, CO_2 , Br_2 , HBr, H_2O
200	CH_2Br_2 , CO, CO_2 , Br_2 , HBr, H_2O
225	CH_2Br_2 , CO_2 , HBr, Br_2 , H_2O
250	CO_2 , HBr, Br_2 , H_2O
275	CO_2 , HBr, Br_2 , H_2O
300	CO_2 , HBr, Br_2 , H_2O

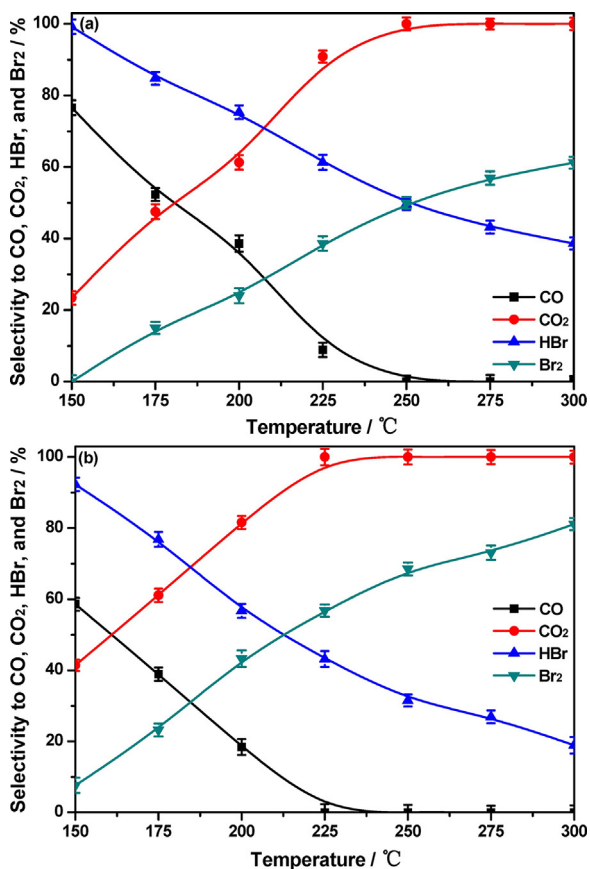


Fig. 7. Selectivities to CO, CO₂, Br₂ and HBr as a function of temperature over Co₃O₄ (a) and Co-Mn-Ti (b) catalysts.

at each evaluated temperature. The selectivity to Br₂ reaches 81% at 300 °C. These results indicate that the addition of Mn and Ti to Co₃O₄ favors the deep oxidation of CO to CO₂ and promotes the generation of Br₂.

The effect of water and PX

It is essential to investigate the effect of water on the CH₂Br₂-oxidation activity of these catalysts, because water is usually present in BVOCs-containing industrial exhaust gas. As shown in Fig. 8, CH₂Br₂ conversion over Co₃O₄ and Co-Mn-Ti at various temperatures was investigated in the presence of 2 vol% H₂O. The results show that CH₂Br₂ conversion over Co₃O₄ and Co-Mn-Ti is improved at low temperature compared with the results without water, and T₁₀ (the temperature needed for 10% conversion) decreases by 10–15 °C. The enhancing effect of water with Co₃O₄ and Co-Mn-Ti on CH₂Br₂ oxidation might be due to the removal of surface bromine species based on the reverse Deacon reaction, i.e., H₂O + Br⁻ ⇌ HBr + OH⁻ [30]. However, with an increase in temperature, a remarkable decrease in CH₂Br₂ conversion is observed, and T₉₀ shifts to higher temperature. This is ascribed to competitive adsorption between H₂O and CH₂Br₂ at the active sites.

It is well known that BVOCs-containing industrial exhaust gas contains various organic compounds, but it is impossible to investigate the effect of different organic compounds on CH₂Br₂ oxidation simultaneously. Consequently, we studied the reaction behaviors referring to a binary mixture of organic compounds, and the effect of PX as a model PTA-exhaust-gas organic compound on the activity of the catalysts for CH₂Br₂ oxidation was investigated. As shown in Fig. 8, the T₉₀ values over Co₃O₄ and Co-Mn-Ti in the

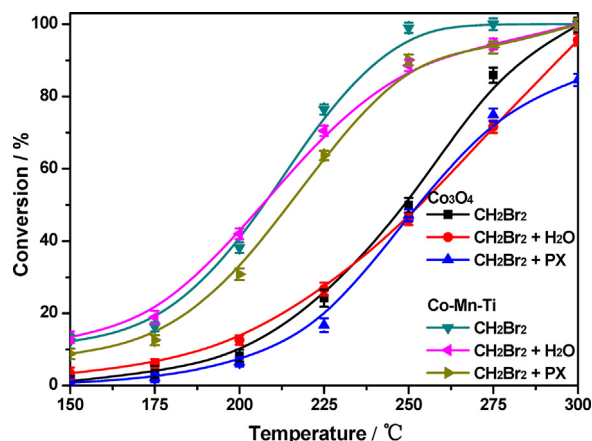


Fig. 8. The effect of water and PX on CH₂Br₂ oxidation over Co₃O₄ and Co-Mn-Ti catalysts; CH₂Br₂ alone: 500 ppm CH₂Br₂; CH₂Br₂ + H₂O: 500 ppm CH₂Br₂ + 2 vol% H₂O; CH₂Br₂ + PX: 500 ppm CH₂Br₂ + 500 ppm PX; in all cases, 10% O₂ and N₂ balance; GHSV = 60,000 h⁻¹.

presence of PX are 311 and 270 °C, respectively, which are slightly higher compared with the results in the absence of PX (287 and 234 °C). This inhibiting effect may be ascribed to a decrease in the number of active sites owing to their consumption by PX oxidation.

Catalyst stability

Catalyst deactivation is the main problem that urgently requires addressing for the practical application of these kinds of catalysts, so it is very important to investigate catalyst stability. The stability experiments were conducted by feeding a stream containing 500 ppm CH₂Br₂, 10% O₂, and N₂ balance at 250 °C and a GHSV of 60,000 h⁻¹, and the results for Co₃O₄, Co-Mn, Co-Ti, and Co-Mn-Ti are shown in Fig. 9. Stable activity is exhibited over 30 h by Co₃O₄, Co-Mn, Co-Ti, and Co-Mn-Ti, with CH₂Br₂ conversions of approximately 49, 77, 98, and 99%, respectively. During the stability test, the selectivities to CO, CO₂, HBr, and Br₂ remain almost constant, revealing that the structure and surface composition of the active sites are stable. It is generally thought that the accumulation of Br species on Co₃O₄-based catalysts is the main reason for loss in activity. XPS analysis showed that the Br contents deposited onto the surfaces of Co₃O₄, Co-Mn, Co-Ti, and Co-Mn-Ti are 1.07, 1.02, 0.89, and 0.81%, respectively, after 30 h reaction at 250 °C. This result indicates that the addition of Mn and Ti to Co₃O₄ promotes the removal of Br species from the surface and improves catalyst stability.

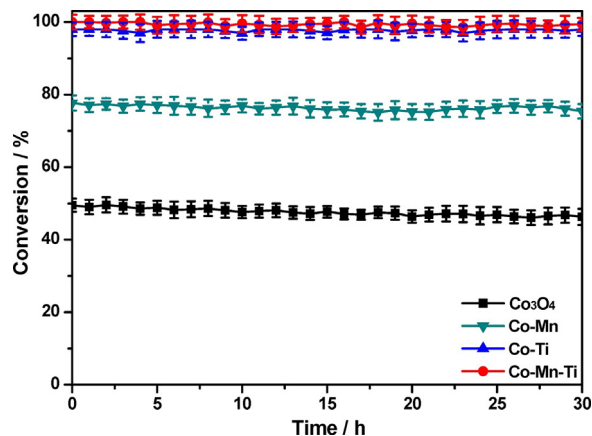


Fig. 9. Stability test of Co₃O₄, Co-Mn, Co-Ti, and Co-Mn-Ti catalysts at 250 °C.

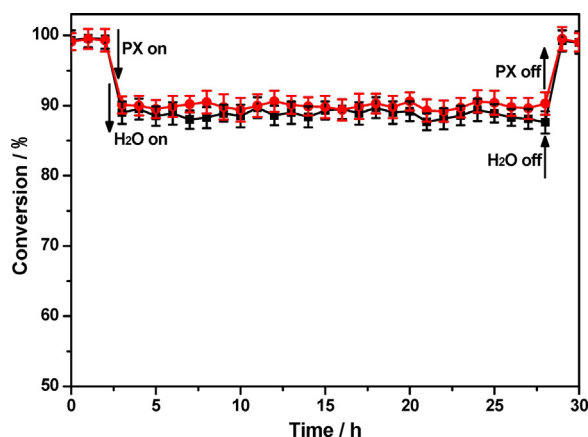


Fig. 10. Stability test of Co-Mn-Ti in the presence of 2 vol% H₂O and 500 ppm PX for CH₂Br₂ oxidation at 250 °C.

We also investigated the stability of Co-Mn-Ti for CH₂Br₂ oxidation in the presence of 2 vol% H₂O and 500 ppm PX at 250 °C. As shown in Fig. 10, CH₂Br₂ conversion stabilizes at approximately 99% within the first 2 h. Next, when 2 vol% H₂O is introduced, there is an obvious decrease in CH₂Br₂ conversion from 99 to 89%, after which conversion remains stable for 26 h, illustrating that H₂O has an inhibitory effect on CH₂Br₂ oxidation by occupying the active sites of the catalyst. When H₂O is removed from the stream, CH₂Br₂ conversion recovers to 99%. This phenomenon indicates that there is a competitive adsorption relationship between CH₂Br₂ and H₂O at the catalyst surface. A similar phenomenon is also observed when 500 ppm PX is introduced. The above results show that Co-Mn-Ti exhibits excellent stability for long-term CH₂Br₂ oxidation, whether in the presence of H₂O or PX, making it suitable for practical application.

In situ DRIFTS study

In order to further explore the intermediate species formed on the catalyst surface, *in situ* DRIFTS experiments were performed, and the results are shown in Fig. 11 (DRIFTS spectra of Co-Mn and Co-Ti are shown in Fig. S4). As shown in Fig. 11(a), after pure Co₃O₄ is exposed to a gas stream containing 500 ppm CH₂Br₂, 10% O₂, and N₂ at 50 °C for 1 h, bands at 3078, 2998, 1620, and 1200 cm⁻¹ are observed. The bands at 3078, 2998, and 1200 cm⁻¹ correspond to methylene (—CH₂—) antisymmetric stretching, symmetric stretching, and wagging, respectively [31], and are appropriate for CH₂Br₂ molecules adsorbed on the surface of Co₃O₄. With an increase in temperature, the bands ascribed to CH₂Br₂ molecules decreased in intensity and are not observed above 100 °C, indicating either their desorption or reaction. The band at 1620 cm⁻¹ is attributed to H₂O on the catalyst surface [32], and disappears at elevated temperature. The disappearance of the bands corresponding to CH₂Br₂ molecules is accompanied by the appearance of new bands at 1541, 1433, and 1348 cm⁻¹, which are related to asymmetric vibration, δ (CH₂), and symmetric vibration of adsorbed formate species (—COOH), respectively [32]. When the temperature exceeds 350 °C, no bands are observed, indicating that CH₂Br₂ is oxidized completely. All of the bands form in the process of CH₂Br₂ oxidation, meaning that formate species are the main intermediate products generated on the surface of Co₃O₄.

For Co-Mn-Ti (Fig. 11(b)), with an increase in temperature, new bands at 1585, 1373, and 1356 cm⁻¹, which are ascribed to COO and CH stretching of adsorbed formate species (—COOH) [33,34], are observed. These results indicate that formate species are the main

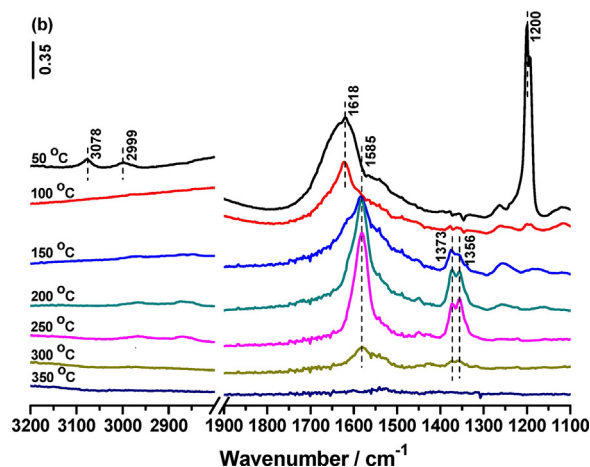
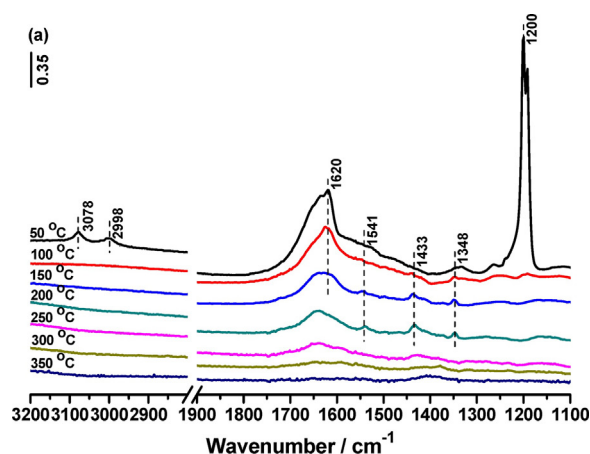


Fig. 11. *In situ* DRIFTS spectra of CH₂Br₂ oxidation over Co₃O₄ (a) and Co-Mn-Ti (b) catalysts at different temperatures.

intermediate products generated on the surface of Co-Mn-Ti, and that the reaction pathway is not significantly changed by the addition of Mn and Ti. Furthermore, no bands related to CO, CO₂, or HBr as the final products are observed, owing to the rapid desorption of these species. Similar phenomena are also observed on the Co-Mn (Fig. S4(a)) and Co-Ti (Fig. S4(b)) catalysts.

Informed by our results, a plausible reaction mechanism for CH₂Br₂ oxidation over Co-Mn-Ti catalysts is proposed, as shown in Fig. 12: (1) CH₂Br₂ adsorbs onto Co species as active acid sites

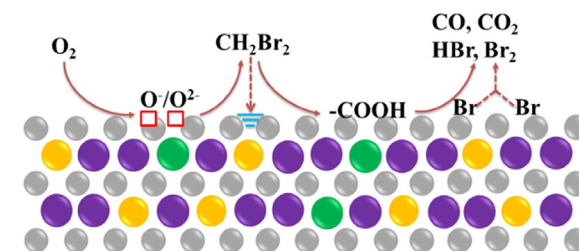


Fig. 12. A plausible reaction mechanism for CH₂Br₂ oxidation over Co-Mn-Ti catalysts.

through bromine atoms; (2) the adsorbed CH_2Br_2 dissociates through the breaking of C-Br bonds into intermediate products, such as formate species; (3) gas-phase oxygen adsorbs onto the catalyst surface to replace the consumed oxygen; (4) the intermediate products are further oxidized by active oxygen species into CO and CO_2 ; and (5) the Br species are replaced by active oxygen species, and the adsorbed Br species desorb from the catalyst surface in the form of HBr and Br_2 .

Conclusions

Considering the low activity of pure Co_3O_4 for catalytic oxidation of BVOCs and its deactivation by bromine poisoning, Co_3O_4 catalysts modified with Mn and Ti were prepared by coprecipitation method to form complexes, and were used for catalytic oxidation of CH_2Br_2 as a model molecule for BVOCs. XRD and Raman analyses showed that the addition of Ti or Ti + Mn to Co_3O_4 distorted its crystal structure, led to the formation of Co–O–Ti solid solutions. The addition of Mn enhanced the surface acidity and increased the redox ability of the catalyst. The catalytic activity of Co_3O_4 was significantly improved by adding Ti or Ti + Mn. The Co–Mn–Ti catalyst exhibited the highest activity, with T_{90} of approximately 234°C and the highest selectivity to CO_2 at low temperature. Additionally, Co–Mn–Ti showed good stability for at least 30 h at 500 ppm CH_2Br_2 , 0 or 2 vol% H_2O , 0 or 500 ppm PX, and 10% O_2 at a GHSV of $60,000\text{ h}^{-1}$, and the final products were CO_x , Br_2 , and HBr, without the formation of other Br-containing organic byproducts. The high catalytic activity was attributed to the high specific surface area, high surface acidity, and strong redox property of the catalyst. Furthermore, the synergetic effect of Co, Mn and Ti promoted the activity of the catalyst for CH_2Br_2 oxidation. *In situ* DRIFTS study showed that formate species are the main intermediate products generated on the surface of Co–Mn–Ti, and a plausible reaction mechanism for CH_2Br_2 oxidation over Co–Mn–Ti catalyst was proposed.

Acknowledgements

This work was supported by the Major State Basic Research Development Program of China (973 Program, No. 2013CB430005), the National Natural Science Foundation of China (No. 51278294 and 21607102), and China's Post-doctoral Science Fun (No. 2015M581626).

Appendix A. Supplementary data

Supplementary data associated with this article can be found, in the online version, at <http://dx.doi.org/10.1016/j.jiec.2017.08.025>.

References

- [1] J. Kan, L. Deng, B. Li, Q. Huang, S. Zhu, S. Shen, Y. Chen, *Appl. Catal. A: Gen.* 530 (2016) 21.
- [2] Q. Dai, W. Wang, X. Wang, G. Lu, *Appl. Catal. B: Environ.* 203 (2017) 31.
- [3] W. Wang, Q. Zhu, Q. Dai, X. Wang, *Chem. Eng. J.* 307 (2016) 1037.
- [4] X. Huang, *Environ. Eng.* 29 (2011) 98.
- [5] X.X. Hao, H.Z. Wang, X.N. Wang, X. Wang, Z.S. Liu, *Contemp. Chem. Ind.* 2 (2013) 020.
- [6] X. Liu, J. Zeng, J. Wang, W. Shi, T. Zhu, *Catal. Sci. Technol.* 6 (2016) 4337.
- [7] J. Mei, S. Zhao, W. Huang, Z. Qu, N. Yan, *J. Hazard. Mater.* 318 (2016) 1.
- [8] C.Y. Chen, J.J. Pignatello, *Appl. Catal. B: Environ.* 142–143 (2013) 785.
- [9] F.F. Liu, X. Chen, J.H. Tang, M.F. Cui, X. Qiao, *J. Nanjing Univ. Technol. (Nat. Sci. Ed.)* 32 (6) (2010) 31.
- [10] J. Mei, S. Zhao, H. Xu, Z. Qu, N. Yan, *RSC Adv.* 6 (2016) 31181.
- [11] Y. Wang, H. Sun, H.M. Ang, M.O. Tade, S. Wang, *Chem. Eng. J.* 245 (2014) 1.
- [12] C. Wang, C. Zhang, W. Hua, Y. Guo, G. Lu, S. Gil, A. Giroir-Fendler, *Chem. Eng. J.* 315 (2017) 392.
- [13] Y. Liao, X. Zhang, R. Peng, M. Zhao, D. Ye, *Appl. Surf. Sci.* 405 (2017) 20.
- [14] E. Saputra, S. Muhammad, H. Sun, H.M. Ang, M.O. Tade, S. Wang, *Appl. Catal. B: Environ.* 154–155 (2014) 246.
- [15] T. Cai, H. Hao, D. Wei, Q. Dai, L. Wei, X. Wang, *Appl. Catal. B: Environ.* 166–167 (2015) 393.
- [16] J. Li, X. Liang, S. Xu, J. Hao, *Appl. Catal. B: Environ.* 90 (2009) 307.
- [17] S. Cao, H. Wang, M. Shi, S. Chen, Z. Wu, *Catal. Lett.* 146 (2016) 1591.
- [18] H. Sun, Y. Bai, H. Liu, W. Jin, N. Xu, G. Chen, B. Xu, *J. Phys. Chem. C* 112 (2008) 13304.
- [19] J. Mei, Y. Ke, Z. Yu, X. Hu, Z. Qu, N. Yan, *Chem. Eng. J.* 320 (2017) 124.
- [20] H. Du, C. Yuan, K. Huang, W. Wang, K. Zhang, B. Geng, *J. Mater. Chem. A* 5 (11) (2017) 5342.
- [21] C. Shi, Y. Wang, A. Zhu, B. Chen, C. Au, *Catal. Commun.* 28 (2012) 18.
- [22] S. Zhang, M. Ye, A. Han, C. Liu, *Appl. Phys. A* 122 (2016) 1.
- [23] V.G. Hadjiev, M.N. Iliev, I.V. Vergilov, *J. Phys. C: Solid State Phys.* 21 (2000) 199.
- [24] S. Yuvaraj, R.H. Vignesh, L. Vasylechko, Y.S. Lee, R.K. Selvan, *RSC Adv.* 6 (2016) 69016.
- [25] G. Weber, A. Vogel, *Polyhedron* 28 (2009) 579.
- [26] C. Zhang, L. Zhang, G.C. Xu, X. Ma, Y.H. Li, C. Zhang, D. Jia, *New J. Chem.* 41 (2017) 1631.
- [27] C. Yu, B. Huang, L. Dong, F. Chen, Y. Yang, Y. Fan, Y. Yang, X. Liu, X. Wang, *Chem. Eng. J.* 316 (2017) 1059.
- [28] L. Li, Y. Yao, Z. Tang, W. Ji, Y. Dai, X. Shen, *J. Nanosci. Nanotechnol.* 16 (2016) 7573.
- [29] C.Y. Chen, J.J. Pignatello, *Appl. Catal. B: Environ.* 142–143 (2013) 785.
- [30] C.E. Hetrick, F. Patcas, M.D. Amiridis, *Appl. Catal. B: Environ.* 101 (2011) 622.
- [31] M.T. Chen, C.F. Lien, A. Lifan Liao, J.L. Lin, *J. Phys. Chem. B* 107 (2003) 3837.
- [32] Y. Wang, A.P. Jia, M.F. Luo, J.Q. Lu, *Appl. Catal. B: Environ.* 165 (2015) 477.
- [33] J. Su, W. Yao, Y. Liu, Z. Wu, *Appl. Surf. Sci.* 396 (2016) 1026.
- [34] C. Shuang, W. Haiqiang, Y. Feixiang, S. Mengpa, C. Shuang, W. Xiaole, L. Yue, W. Zhongbiao, *J. Colloid Interface Sci.* 463 (2016) 233.